Inductive coupling on metallic pipelines: Effects of a nonuniform soil resistivity along a pipeline-power line corridor

(Article begins on next page)

06 October 2024

Inductive coupling on metallic pipelines: effects of a nonuniform soil resistivity along a pipeline-power line corridor

Arturo Popoli[a,*], Leonardo Sandrolini[a], Andrea Cristofolini[a]

[a]*Department of Electrical, Electronic, and Information Engineering, University of Bologna, Bologna, 40136, Italy*

Abstract

Metallic buried pipelines sharing the same corridor with AC power lines are subjected to AC interference, potentially harmful to personnel and equipment. The inductive coupling depends, among other factors, on the physical characteristics of the soil. This work presents an analysis of the effects of soil resistivity nonuniformities spanning along the length of a corridor. The investigation is performed by assessing several realistic configurations suited to highlight the various mechanisms affecting the phenomenon. The calculations are carried out employing an ad-hoc developed numerical tool, where the network analysis is used to enforce physical constraints on a 2D finite element analysis. The obtained results show that longitudinal nonuniformities in the soil resistivity can significantly affect the induced currents, depending on the particular configuration of the power line under exam.

Keywords: AC Interference, Pipeline, Inductive Coupling, Finite Element Method, Soil Resistivity

1. Introduction

The process of transporting water, oil and gas is generally performed by means of metallic pipelines buried in the soil. For several reasons, such as high

---

*Corresponding author
Email address:* `arturo.popoli@unibo.it` (Arturo Popoli)

costs of land and environmental concerns, these structures often share their geographical corridors with high voltage AC (HVAC) power lines. A metallic pipeline located in the proximity of a HVAC power line will inevitably experience inductive coupling due to the power line currents [1]. Although AC interference to pipelines is commonly regarded as less severe than DC current interference, if the values of the induced voltages and currents on a pipeline exceed certain threshold levels, the pipeline's risk of experiencing electrochemical corrosion is considered to be high [2, 3]. Likewise, whenever the induced pipeline voltage with respect to the remote earth is higher than $50 - 60$ V, workers touching the pipeline are exposed to electrical shock [4, 5]. Finally, high levels of induced voltages can result in damages for the active cathodic protection systems connected to the pipeline. For the above reasons, an accurate knowledge of these phenomena is fundamental for the design of pipelines routings and mitigation measures for existing structures [6, 7]. In this spirit, the necessity of reliable simulation tools for the assessment of the induced electromagnetic variables on buried pipelines stems from both the inherent complexity of the problem and the technical difficulty of performing measurements on such wide geometries.

The majority of the calculation methodologies devoted to the study of AC interference on metallic objects use the transmission line theory for the assessment of the inductive coupling [8–10]. As discussed in [11], these techniques are generally based on approximate formulas [12, 13] for the evaluation of the mutual impedance between earth-return conductors. These are employed to overcome the computational cost of a direct solution of the Carson [14] and Pollaczek integrals [15]. Nevertheless, Finite Element Analysis (FEA) is also applicable to the task of AC interference. The quasi-3D methodology introduced in [16, 17] employs a series of 2D finite element simulations to extract the physical dependencies existing among the different conductors of a given corridor section. The obtained information can be embedded in an equivalent electrical circuit, which serves the purpose of enforcing appropriate constraints on the electromagnetic quantities, complementing the assumptions made when

the 2D FEA is performed. In this way, the developed methodology allows imperfect coatings or groundings of the metallic conductors to be modelled in a physically consistent way, while retaining the advantages provided by the employment of a FEA.

In this work, the above described quasi-3D methodology is employed to perform a study on the influence of longitudinal nonuniformities of the soil electrical resistivity over the induced voltages and currents on the pipeline. Variations of the soil resistivity, in fact, may yield unsafe touch voltages on the pipeline, as well as values of current that can lead to electrochemical corrosion [18]. Throughout the years, considerable attention has been devoted to develop mathematical methodologies that could take into account vertically or horizontally stratified soils, both through the extension of existing analytical approaches [19, 20] and implementing methods based on a combination of bidimensional FEA and mesh analysis (hybrid techniques) [21–23]. However, to the authors' best knowledge, the effects caused by gradients of the soil electrical resistivity along a corridor (the z direction of Fig. 1) have not been studied extensively yet. It is worth considering that a change in the value of soil resistivity at one point of the corridor is responsible for two effects that have opposite consequences on the induced electromagnetic fields: the inducing effect of the power line grows with the soil resistivity (due to a less effective screening effect of the soil) but so does the impedance of the earth-return path for the induced currents. The combination of these two opposing effects makes nontrivial the evaluation of their resulting consequences on the pipeline.

This work is focused on the twofold purpose of adapting the quasi-3D methodology introduced in [16, 17] to investigate such interference cases, and to provide an interpretation to the physical effects produced by the aforementioned longitudinal soil nonuniformities. In order to do so, a simple configuration is analyzed using both the developed quasi-3D methodology and the well consolidated approach described in the CIGRE guide [24]. Afterwards, more complex configurations (i.e. adding an overhead ground wire (OGW) and assuming a nonparallel

3

pipeline-power line routing) are investigated, aiming to reproduce more realistic interference cases. The following sections will show that the described changes in soil resistivity can both mitigate or intensify the AC interference induced by a power line on metallic objects sharing the same corridor. This, depending on the geometry and configuration of the considered structures, may result in over-estimations of the induced currents, or unexpected hazardous conditions that need to be carefully assessed in the safety design process for these kind of structures.
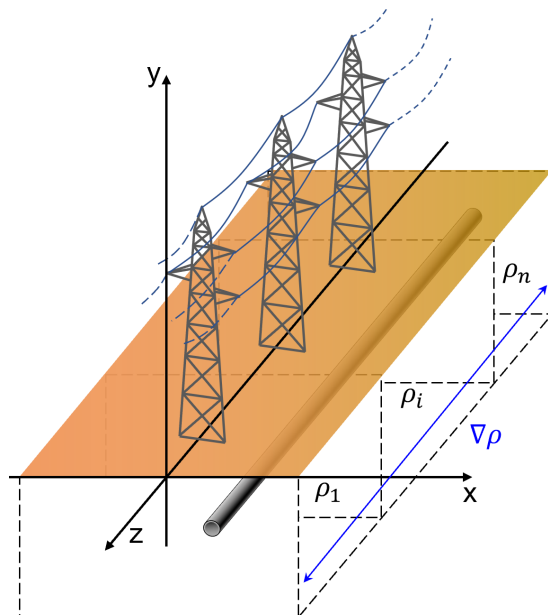

Figure 1: Representation of a corridor with a power line and a metallic pipeline buried in the soil, which features a longitudinal variation of electrical resistivity.

2. Numerical Methodology

The quasi-3D methodology utilized in this paper is based on a 2D FEA, performed on a certain number of sections of the considered power line-pipeline corridor. Each section represents the specific features of the corridor at a given position along the line, i.e., the relative positioning between the pipeline and

4

the power line, the soil characteristics, including nonuniformities and stratifications, the presence of earthing and mitigation devices. The number of sections along the corridor determines the accuracy of the solution along the longitudinal direction. However, the considered sections are not physically independent. A circuital approach is employed to enforce the interconnection between these sections. That is, for each section, FEA is used to extract the parameters of a multiport component, which describes the local behaviour of the corridor in terms of voltage and current. The components obtained in this way are then assembled to form an electrical network that describes the entire corridor.

2.1. Finite element formulation

As previously mentioned, the finite element solver is a fundamental block of the analysis tool developed to obtain the results described in this paper. The solver is based on a quasi-magnetostatic formulation, where only the conduction current is considered in the Ampére-Maxwell law. The voltages and currents are assumed to be in a sinusoidal steady-state, and the materials are considered to be linear and isotropic. Finally, the current densities are assumed to flow perpendicularly to the calculation plane. Hence, if the power line is directed along the z-axis, $\vec{J} = J_z(x, y, t)\hat{k}$, and a magnetic vector potential $\vec{A} = A_z(x, y, t)\hat{k}$ is defined for the magnetic field, such that $\vec{B} = \nabla \times \vec{A}$. These assumptions, discussed in more detail in [16], allow one to formulate the diffusion equation of the magnetic vector potential with the following stationary complex expression:

$$-\nabla \cdot \left(\frac{1}{\mu} \nabla \underline{A_z} \right) = \underline{J_{0,z}} - j\omega\sigma\underline{A_z}, \tag{1}$$

The unknown $\underline{A_z}$ appearing in (1) is the phasor associated to the sinusoidal component A_z of the magnetic vector potential, while the phasor $\underline{J_{0,z}}$ accounts for the impressed current densities due to externally applied fields along the z direction (such as the power line three-phase source). Equation (1) is discretized by means of a finite element approach [25], yielding a complex linear algebraic

system:

$$[\underline{\boldsymbol{K}}]\{\underline{\boldsymbol{A}}_z\} = \{\underline{\boldsymbol{f}}\}, \tag{2}$$

which provides the nodal values of $\underline{A}_z$. The right hand side in (2) takes into account the imposed current densities $\underline{J}_{0,z}$ and the boundary conditions. Thus, (2) can be regarded as an algebraic expression describing the relationship between the forcing terms of the problem (i.e. the impressed current densities $\underline{J}_{0,z}$) and their effects on the considered section, that is, the vector potential distribution. The forcing terms $\underline{J}_{0,z}$ are generally not known *a priori*, since they are related to the longitudinal electric fields, and depend on the behaviour of the whole system. Hence, the problem requires the physical interactions between the considered sections to be modelled. As anticipated, this task is carried out by introducing an circuital model.

2.2. Equivalent circuit

A power line-pipeline corridor with a generic routing can be approximated by a sequence of segments of finite longitudinal length. The FEA described in the previous section is utilised on each of these segments, to derive a linear relation between the forcing terms and the electric currents in each conductor. In symbolic form, the current density due to inductive coupling can be expressed as:

$$\underline{J}_z = \underline{J}_{0,z} - j\omega\sigma\underline{A}_z, \tag{3}$$

where $\underline{J}_{0,z}$ represents the current density corresponding to a stationary problem, i.e., without the self and mutual induction effects, which are accounted with the $-j\omega\sigma\underline{A}_z$ term. The electric current $\underline{I}_h$ in a generic conductor h can therefore be obtained by integrating $\underline{J}_z$ over its cross-section S_h on the $x - y$ domain Ω, as:

$$\underline{I}_h = \int_{S_h} \underline{J}_z \mathrm{d}S = \int_{S_h} \underline{J}_{0,z} \mathrm{d}S - j\omega \int_{S_h} \sigma\underline{A}_z \mathrm{d}S. \tag{4}$$

This allows one to derive a linear relationship between the array $\{\underline{I}\}$ composed of the electric currents $\underline{I}_1, \underline{I}_2, \ldots, \underline{I}_n$ in each conductor of the considered sec-

tion, and the forcing term array $\{\underline{J}_{z,0}\}$, whose entries are the impressed current densities $\underline{J}_{z,0,1}$, $\underline{J}_{z,0,2}$, ..., $\underline{J}_{z,0,n}$ on the conductors:

$$\{\underline{I}\} = [\underline{M}]\{\underline{J}_{z,0}\}. \tag{5}$$

Equation (5) can be considered as a definition of the characteristic matrix $[\underline{M}]$. In a system with n conductors (including OGWs and the soil), the characteristic matrix $[\underline{M}]$ is a rank n complex square matrix embodying the relationship between the conductors due to the phenomenon of electromagnetic induction. The generic entry $m_{h,k}$ of $[\underline{M}]$ is the current $\underline{I_h}$ flowing through the hth conductor when a unit current density $\underline{J_{0,z,k}}$ is enforced on the kth one. As a result, the characteristic matrix is populated by running n FEM simulations, in each of which all the entries in $\underline{J_{z,0}}$ are set to zero, except for $\underline{J_{0,z,k}}$ which assumes unit value. The values of the kth column of $[\underline{M}]$ are found by calculating the current on the conductors according to (4).

Considering a segment of corridor with a longitudinal length L_s, the $\underline{J_{z,0,k}}$ impressed current acting on the kth conductor is related to the voltage $\underline{V_k}$ applied to the same conductor along its longitudinal length by:

$$\underline{J_{z,0,k}} = \frac{\sigma_k}{L_s}\underline{V_k}. \tag{6}$$

Therefore, it is possible to derive from (5) and (6) a constitutive relation of an n-port circuit component representing the behaviour of a corridor segment as obtained from FEA. Fig. 2 shows the first two cells of an equivalent circuit encompassing the derived n-port components with the above described methodology (the third phase conductor has been omitted for the sake of clarity). As one can see, every cell features an admittance connecting the OGW to the soil, in order to account for the combined impedances of the power tower metallic structure and groundings. As the present work does not feature any fault condition, the line conductors' admittances have not been considered (hence omitted in Fig. 2). Nevertheless, a fault involving a current running from a line conductor to the soil through the power tower can be simulated as well, as long as the assumption of a sinusoidal steady-state is valid. This can be done by connecting

7

the faulted line conductor to the soil via an impedance, representing the sum of the pylon and the power tower grounding system impedances. In Sec. 3, two different routings of the pipeline are considered, as well as two different soil structures. The general case of a pipeline crossing the power line in presence of longitudinal nonuniformities of the soil resistivity is treated by subdividing the corridor in a series of sections, in which the pipeline is considered to be (locally) parallel to the power line. In this way, the condition $\vec{J} = J_z(x, y, t)\hat{k}$ is always fulfilled. Each section is associated with a set of electrical properties and a 2D domain discretization, constituting the input of the finite element solver. For every section, the aforementioned characteristic matrix is extracted via the FEA, and the resulting equivalent electric network is solved via standard tableau analysis technique, as detailed in [16].
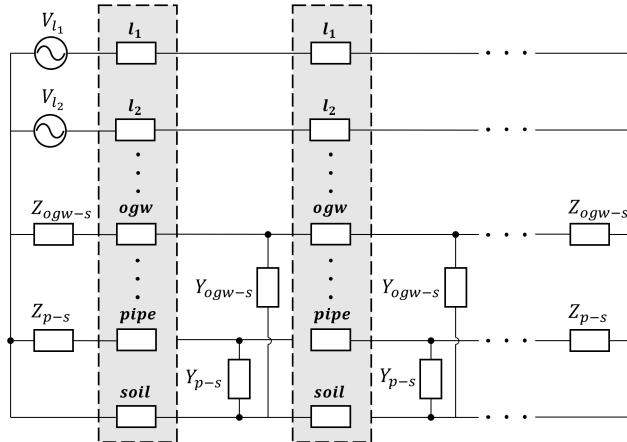

Figure 2: Schematic of the equivalent network embodying the characteristic matrices.

3. Results and Discussion

In the next paragraphs, the following four corridor configurations are analysed, focusing on the effects of longitudinal soil nonuniformities:

(A) Pipeline running parallel to a power line without OGW;

(B) Pipeline running parallel to a power line with a single OGW;

8

(C) Pipeline crossing a power line without OGW (nonparallel routing);

(D) Pipeline crossing a power line with a single OGW (nonparallel routing).

In the listed configurations, soil resistivity nonuniformities on the xy plane of Fig. 1 have purposely not been included, in order to focus on the effects of the ones along the z direction, along the corridor. Figure 3 shows the geometrical disposition of the power line conductors, which, together with the pipeline burial depth, is retained for all the considered configurations. Other geometrical and electrical properties of the line conductors, pipeline, soil and OGWs are reported in Tab. 1, along with relevant references. The adopted values for the pipeline and OGW electrical properties correspond to steel and aluminium, respectively. The pipeline per unit length admittance to soil $y_{p,s}$ has been evaluated with the expression provided in [24], assuming a 5 mm thick bituminous coating resistivity of $\rho = 2 \times 10^6 \, \Omega \, \text{m}$ and $\epsilon_r = 5$. The value for the OGW admittance to the soil conductor (y'_{ogw-s}) has been obtained assuming that a power tower is installed every 200 m of the power line, and that the series of every power tower and its grounding system has a resistance of $10 \, \Omega$ [26, 27], giving $Y_{tower} = 0.1 \, \text{S}$. Consequently, the power tower admittance-to-soil is then distributed over 200 m, yielding the p.u.l. value reported in the table. Each of the four listed configurations has been simulated twice, firstly assuming that the pipeline is buried in a uniform soil with $\rho_s = 50 \, \Omega \, \text{m}$ (ρ_u in Fig. 5, then by considering the nonuniform resistivity profile denoted as ρ_{nu} in Fig. 5. This latter assumption corresponds to a corridor that crosses different kinds of soil, and hence different values of electrical resistivity. In the resistivity profile depicted in Fig. 5, the lower value of $\rho_s = 50 \, \Omega \, \text{m}$ corresponds to a fairly conductive soil (e.g., clay), while the higher one ($\rho_s = 5 \times 10^3 \, \Omega \, \text{m}$) is typical of gravel or sandstone [24].

3.1. A - Parallel routing without OGW

In this first test (A) the pipeline has been assumed to run parallel to a power line with the geometrical characteristics described in Fig. 3, with the exception of the OGW, which has been excluded. The pipeline horizontal positioning

Table 1: Geometrical and electrical data

| Physical quantity	Value	
$I_{l,I}$ (line current) [28]	$600\underline{/0°}$	A
$I_{l,II}$	$600\underline{/-120°}$	A
$I_{l,III}$	$600\underline{/120°}$	A
σ_p (pipe electr. conductivity)	5.5×10^6	$\mathrm{S\,m^{-1}}$
$r_{ext,p}$ (pipe external radius)	0.5	m
$r_{int,p}$ (pipe internal radius)	0.475	m
$\mu_{r,p}$ (pipe rel. magnetic perm.)	250	$-$
y'_{p-s} (pipe admitt. to earth) [24]	3×10^{-4}+j9×10^{-6}	$\mathrm{S\,m^{-1}}$
z_{p-s} (pipe terminal imped.)	1	$\mathrm{k\Omega}$
σ_{ogw} (OGW electr. conductivity)	3.77×10^7	$\mathrm{S\,m^{-1}}$
r_{ogw} (OGW radius)	6×10^{-3}	m
y'_{ogw-s} (OGW admitt. to earth)	5×10^{-4}	$\mathrm{S\,m^{-1}}$
z_{ogw-s} (OGW terminal imped.)	1	Ω
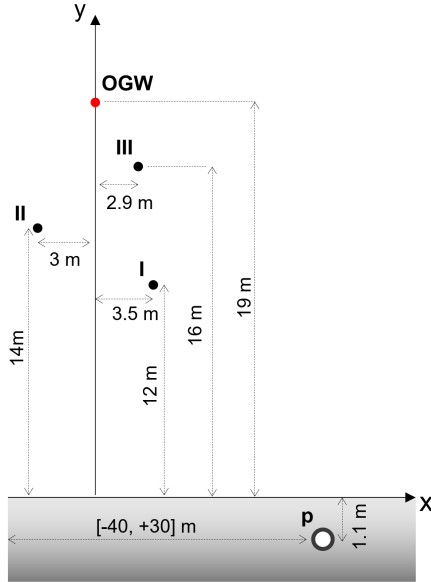
Figure 3: Geometrical positions of the conductors.

with respect to the power line has been set to $h_d = -40\,\text{m}$. With reference to Fig. 4, the negative sign denotes that the pipeline is located on the left of the power line. The information extracted via the quasi-magnetostatic 2D analysis has been used to build an equivalent network as described in Sec. 2.2, consisting of 880 cells representative of $25\,\text{m}$ each, to reach the total corridor length $L = 22\,\text{km}$.

This configuration has been analyzed using both the developed quasi-3D methodology and the procedure prescribed in the CIGRE guide on the influence of high voltage AC power systems on metallic pipelines [24]. The latter represents a well established methodology that can be employed for the validation of the simulation results [29], especially regarding power line configurations without OGWs [11]. Figure 6 shows the obtained pipeline current and pipeline-to-soil voltage for the two cases of uniform and nonuniform longitudinal soils computed using the two different calculation techniques. With a $3.2\,\%$ maximum relative difference in the obtained pipeline current I_p for the uniform soil
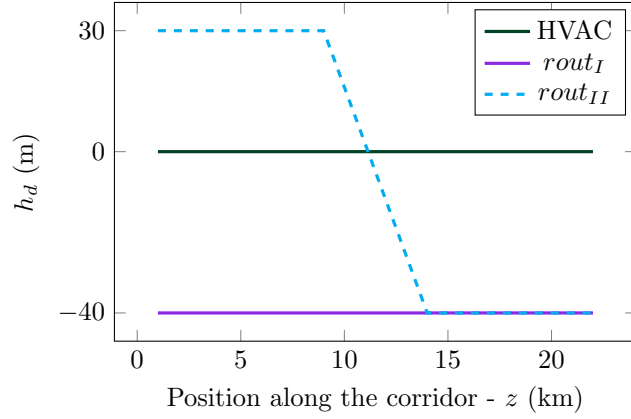
11

Figure 4: Pipeline horizontal positioning with respect to the HVAC power line (h_d) for the parallel ($rout_I$) and oblique routing ($rout_{II}$).
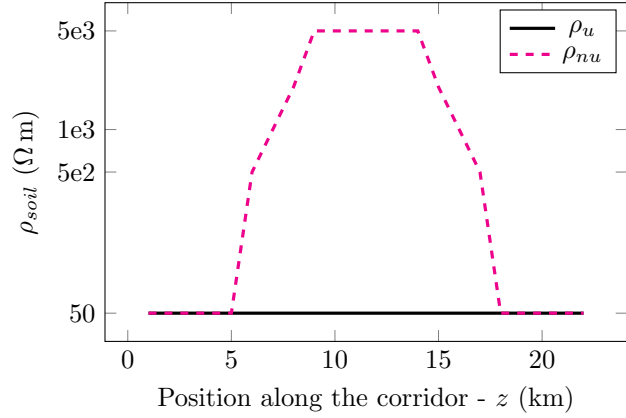

Figure 5: Uniform (ρ_u) and nonuniform (ρ_{nu}) longitudinal soil resistivity profiles employed in the simulations.

case 6 (a), the two approaches show a good agreement for this configuration.

As one can see from Fig. 6 (a), the induced pipeline current decreases by 18.3 % at the midpoint of the corridor ($z = 11\,\mathrm{km}$) when the nonuniform soil structure is considered. The same behaviour of the induced current occurs (with a phase shift of 180°) in the soil. The HVAC transmission line carries a balanced system of currents, i.e., the sum of the line currents is null: $\sum_l I_l = 0$. In absence of other earth-return conductors, the pipeline current can only take the soil as a return path ($I_p + I_s = 0$). An increase of soil resistivity produces two opposing effects with respect to the induced current:

1. The local electromotive force induced on any conductor by the power line is increased, due to a lower screening effect of the soil with regards to the time-varying magnetic field of the power line;

2. Considering a generic earth-return conductor, the real part of the impedance of its return path is increased proportionally to the soil resistivity.

Figure 6 (b) shows the magnitude profile of the obtained pipeline-to-soil voltage. As one can see, the nonuniform soil resistivity profile does not radically change the magnitude of the induced voltage. However, it is worth noticing that the inflection points exhibited by the voltage obtained using ρ_{nu}, i.e, at $z = 5\,\mathrm{km}$ and $z = 17\,\mathrm{km}$ are located where ρ_{soil} changes sharply. Indeed, the *slab* of high soil resistivity has essentially the effect of partially isolating the parts of the pipeline located at its left and right sides. In the hypothetical case of an extremely high resistivity of the soil *slab*, the obtained induced voltage (between $z = 0\,\mathrm{km}$ and $z = 5\,\mathrm{km}$) would show the characteristic V-shaped profile that can be observed between the two ends of the corridor when the uniform soil resistivity is employed ($Q3D$ ρ_u in Fig. 6 b). The same would be true considering the portion of the pipeline between $z = 17\,\mathrm{km}$ and $z = 22\,\mathrm{km}$ in the ρ_u case.

From a technical standpoint, a mitigation system (i.e. a combination of grounding and screening conductors) designed under the assumption of uniform soil (ρ_u in Fig. 6) would not be optimal for the described nonuniform soil resistivity profile. As an example, taking action against the maximum induced

current obtained with ρ_u would lead to installing an insulating joint at $z = 11\,\mathrm{km}$. However, the current profile obtained with ρ_{nu} indicates $z = 7\,\mathrm{km}$ and $z = 15\,\mathrm{km}$ as the two most problematic spots.

3.2. B - Parallel routing with a single OGW

For this second test (B), all the geometrical and electrical parameters (including the pipeline path) are unchanged with respect to test (A), with the exception of the OGW. Indeed, in this test the power line is assumed to comprise an OGW, characterized by a p.u.l admittance to earth of $5 \times 10^{-4}\,\mathrm{S\,m^{-1}}$. The reason for repeating the same test with the only addition of the OGW is that its earth-return nature increases the physical complexity of the phenomena taking place among the various considered conductors. Indeed, the results depicted in Fig. 7 show that the presence of the OGW drastically changes the profile of the induced currents and voltages on the pipeline when the soil is nonuniform. This fact is notable, as the results of test (A) could lead to attribute to the highly resistive *slab* of soil a mitigating effect towards the pipeline. However, the results of Fig. 7 show that the addition of a single OGW is enough to reverse the effects of the soil nonuniformity, which produces now an increase in the maximum value of induced current on the pipeline, as well as a significant distortion of the induced voltage to earth. In order to explain this behaviour, it is useful to compare tests (A) and (B) when a uniform soil is considered: the addition of the OGW changes the magnitude of the induced currents and voltages, but not their profile. This means that the difference between the results of tests (A) and (B) for the case of nonuniform soil can be related to the interaction between the OGW and the soil. In this respect, it is useful to remember that from the perspective of the soil and the pipeline, the OGW constitutes a rather low impedance path that can bridge portions of the soil, and as such provides a preferential way for the currents that would otherwise be forced to flow through the highly resistive *slab* of soil.

Figure 8 depicts the phasors of the earth-return conductors currents considered in Test (B). The current phasors for the Pipeline, OGW and the soil are
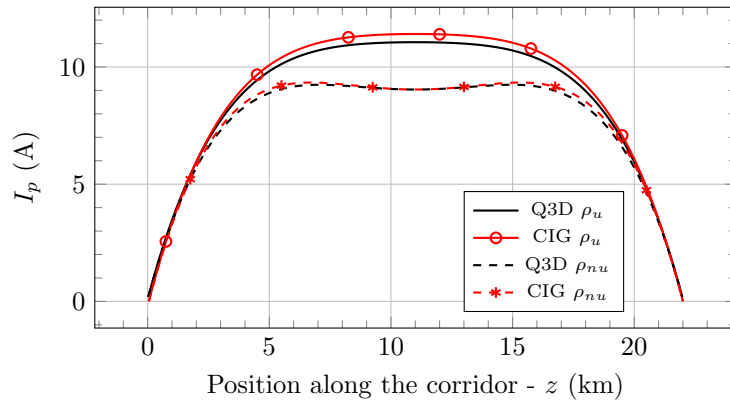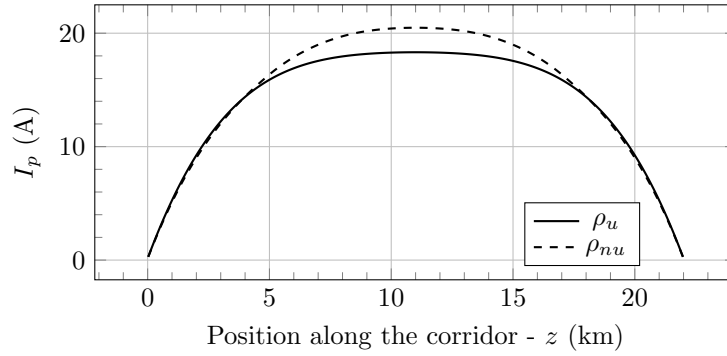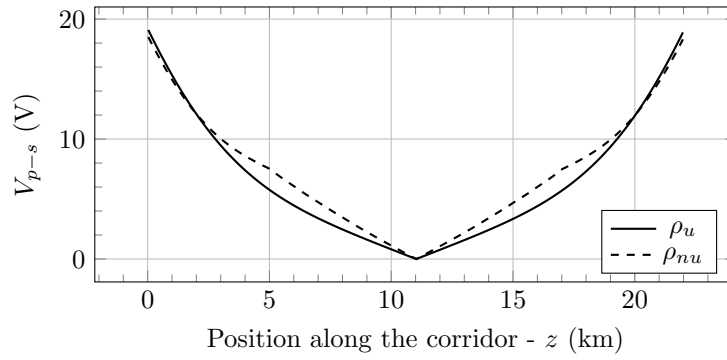
14

(a) Magnitude of induced current on the pipeline
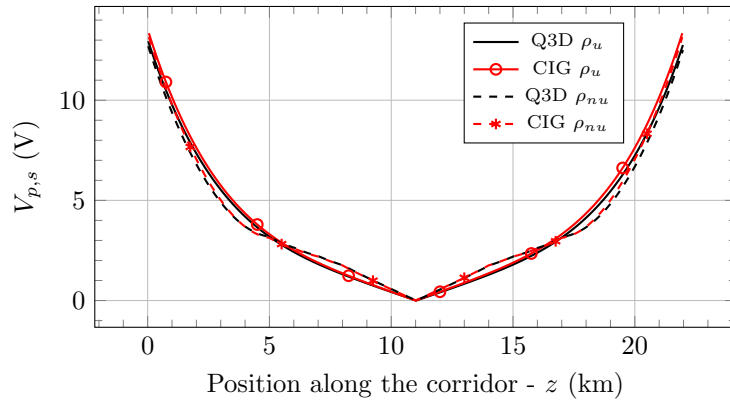
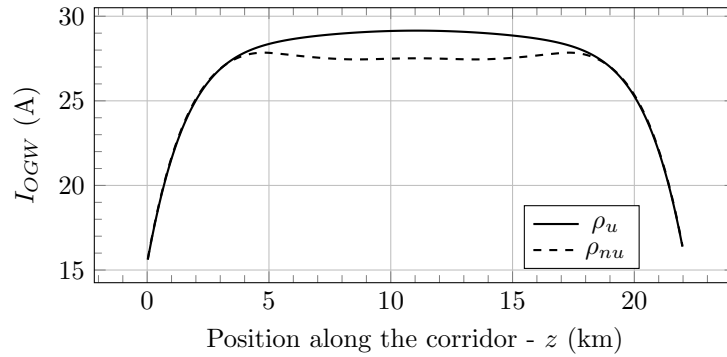
(b) Magnitude of induced voltage-to-earth on the pipeline

Figure 6: Test (A), current and voltage vs corridor position for a pipeline running parallel to a power line ($rout_I$ in Fig. 4) without OGW for the two resistivity profiles shown in Fig. 5: comparison between the quasi-3D methodology (Q3D) and the CIGRE standard (CIG) [24].

(a) Magnitude of induced current on the pipeline.

(b) Magnitude of induced voltage-to-earth on the pipeline.

(c) Magnitude of induced voltage-to-earth on the pipeline.

Figure 7: Test (B), pipeline current, pipeline voltage and OGW current vs corridor position for a pipeline running parallel to a power line ($rout_I$ in Fig. 4) with a single OGW for the two resistivity profiles shown in Fig. 5: results obtained with the quasi-3D methodology.

16

depicted at the midpoint of the corridor (z = 11km), for the two considered longitudinal soil resistivity profiles ρ_u (in Fig. 8a) and ρ_{nu} (in Fig. 8b). The soil resistivity at $z = 11\,\text{km}$ increases from $50\,\Omega\,\text{m}$ (Fig. 8a) to $5 \times 10^3\,\Omega\,\text{m}$ (Fig. 8b). Because of this, each of the three considered currents changes its magnitude and phase:

1. I_s: the magnitude of the soil current decreases from $16.5\,\text{A}$ to $11.9\,\text{A}$ $(-27\,\%)$. This is due to the increase in the soil impedance caused by the higher soil resistivity;

2. I_{OGW}: the increased soil resistivity has a limited effect on the OGW current, which undergoes a $-5\,\%$ decrease, from $29.1\,\text{A}$ to $27.5\,\text{A}$. This is partly because the OGW is an overhead conductor, and hence is not affected by the soil's screening properties;

3. I_p: regarding the pipeline, in Test (B) the OGW is connected to ground at each power tower for the whole length of the right-of-way. Likewise, the pipeline is also connected to the soil over the length of the corridor via its imperfect coating, represented in Fig. 5 (for every cell) as an admittance to earth. Since the line conductors carry a balanced systems of currents, the sum of the three represented currents (I_p, I_s and I_{OGW}) must be null. As I_{OGW} shows only a small change when the ρ_{nu} profile is considered, the observed reduction in the soil current I_s must be balanced out by the pipeline current. Indeed, I_p increases from $18.3\,\text{A}$ to $20.5\,\text{A}$ $(12\,\%)$ from Fig. 8a to Fig. 8b.

3.3. C - Nonparallel routing without OGW

Test (C) differs from the previous two because a nonparallel pipeline-power line routing is considered. In particular, the pipeline follows the dashed path depicted in Fig. 4, denoted as $rout_{II}$. As for the previous tests, the simulations are repeated twice, firstly assuming a uniform soil resistivity of $50\,\Omega\,\text{m}$ (ρ_u), and then the nonuniform soil resistivity profile marked as ρ_{nu}. In order to extract the characteristic matrices needed for the equivalent network construction, 27
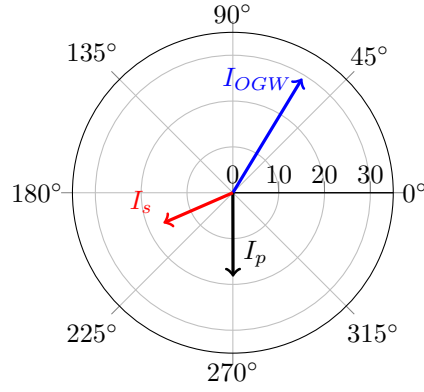
(a) uniform soil - ρ_u
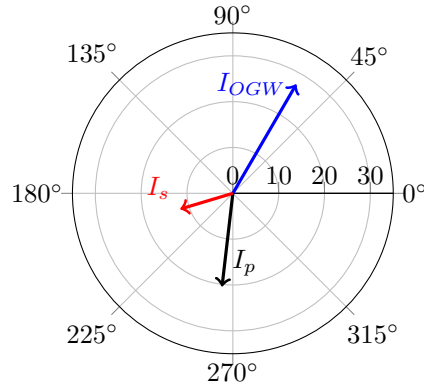
(b) nonuniform soil - ρ_{nu}

Figure 8: Magnitude and phase of the induced currents for test (B) at $z = 11\,\text{km}$.

different 2D meshes have been computed by progressively changing the horizontal distance of the pipeline from the power line centre and the soil electrical resistivity. Figure 9 shows the obtained current and voltage magnitude profiles on the pipeline (for the two considered soil resistivity profiles). As in Test (A), the configuration has been assessed using both the developed quasi-3D code and the methodology prescribed in [24], denoted as *CIG* in the legend of Fig. 9. The results yielded by the two different approaches show a good agreement for both the induced current and voltage. Unlike the results of tests A and B, which refer to parallel configurations, the induced pipeline current profile in Fig. 9 is asym-

metric with respect to the point where the pipeline path crosses the power line, i.e., at $z = 11\,\mathrm{km}$. This can be explained considering that the two upstream and downstream sections of the pipeline with respect to the crossing are not at the same distance from the power line conductors. Indeed, higher values of induced current can be observed on the left of the crossing in Fig. 9, where $|h_d| = 30\,\mathrm{m}$ with respect to the right part of the corridor, where $|h_d| = 40\,\mathrm{m}$. In analogy to what can be observed in Test (A), the ρ_{nu} soil resistivity profile yields a lower maximum value of induced current with respect to the uniform resistivity profile ρ_u. In general, however, the obtained profiles of current and voltage to earth in Fig. 9a and Fig. 9b show that the different routing (with respect to the parallel routing configuration) has a dominant effect with respect to the soil longitudinal nonuniformities. Nevertheless, in this case the maximum value of induced current $I_{p,max}$ is reduced by $10.3\,\%$ when ρ_{nu} is considered, showing a non negligible effect of the longitudinal soil nonuniformity. For the sake of reference, $I_{p,max}$ was reduced by $16.4\,\%$ in the parallel configuration considered for Test A.

3.4. D - Non-parallel routing with a single OGW

Figure 10 shows the results obtained when a single OGW is added to the power line, while keeping the same routing employed for Test (C). Coherently to what has been observed comparing Test (A) to Test (B), the addition of a single OGW to the geometry employed for Test (C) radically changes the effects produced on the pipeline by the nonuniform soil resistivity profile. Indeed, Fig. 10a shows that the nonuniform soil causes now the induced current on the pipeline to rise slightly, as opposed to what has been shown in Fig. 9a. For what concerns the induced voltage, the comparison between Fig. 10b and Fig. 9b highlights that (excluding the two endings of the corridor), the presence of the OGW does not significantly alter the profile of induced voltage. Finally, Fig. 10c confirms what has been observed in Test (B), i.e., that where the soil resistivity is higher the OGW locally acts as a return path for the pipeline current.
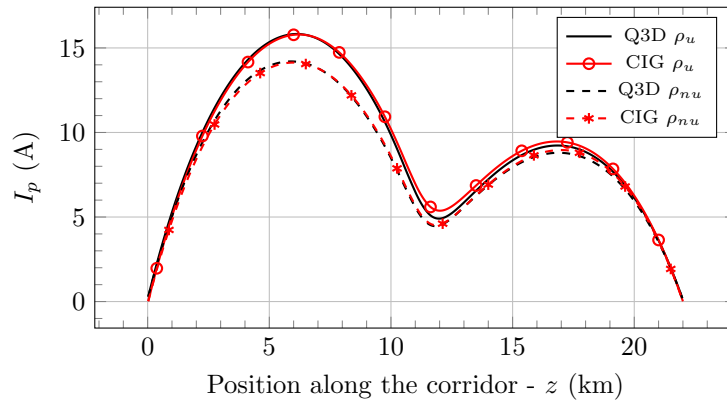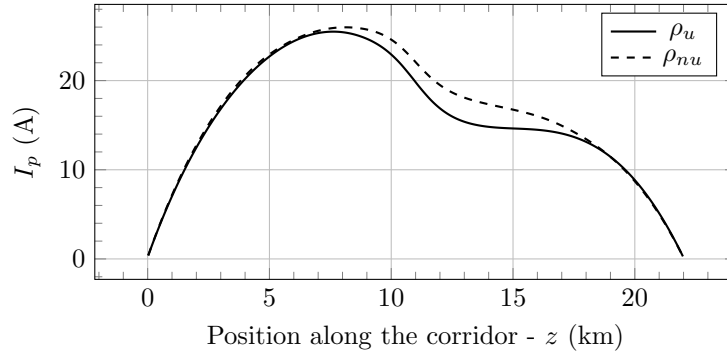
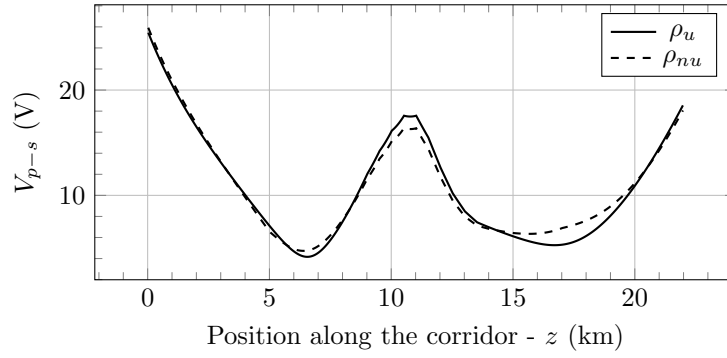(a) Magnitude of induced current on the pipeline
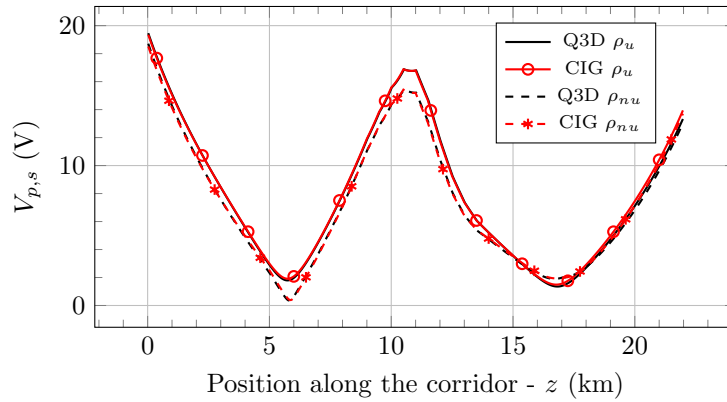
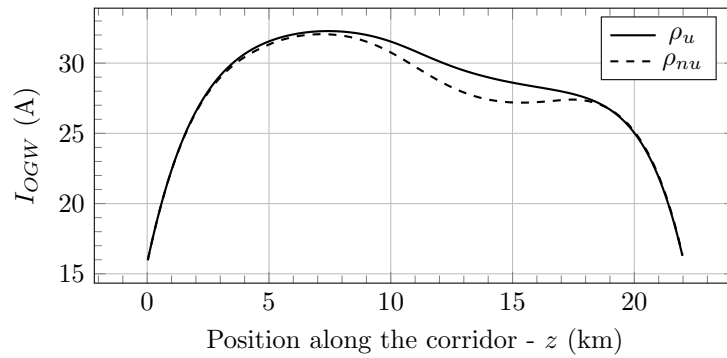(b) Magnitude of induced voltage-to-earth on the pipeline

Figure 9: Test (C), current and voltage vs corridor position for a pipeline crossing a power line ($rout_{II}$ in Fig. 4) without OGW for the two resistivity profiles shown in Fig. 5: comparison between the quasi-3D methodology (Q3D) and the CIGRE standard (CIG) [24].

(a) Magnitude of induced current on the pipeline

(b) Magnitude of induced voltage-to-earth on the pipeline

(c) Magnitude of induced current on the OGW

Figure 10: Test (D), pipeline current, pipeline voltage and OGW current vs corridor position for a pipeline crossing a power line ($rout_{II}$ in Fig. 4) with a single OGW for the two resistivity profiles shown in Fig. 5: results obtained with the quasi-3D methodology.

4. Domain discretization and code performances

The 2D triangular meshes employed for this work consist of circular cross-sections with a radius of 25 km, with the boundary condition $\underline{\boldsymbol{A}}_{\boldsymbol{z}} = \boldsymbol{0}$ enforced on the outer edge. The power line is contained in the upper half of the circular domain, whereas the pipeline is buried in the soil (bottom half). The employed radius has been selected in order to be larger than the magnetic field penetration depth for the highest soil resistivity among the different employed values, i.e., $5000\,\Omega\,\mathrm{m}$. The geometrical sizes of the elements range from hundreds of meters (outer edge of the domain) to sub-millimetric lengths (pipeline, power line conductors), in order to adequately account for the skin effect phenomenon while keeping a reasonable number of nodes. To do so, the outer part of the metallic conductors has been discretized by means of structured regions (offering fine control on the local mesh size), while unstructured Delaunay triangulation has been employed for the rest of the geometry. The meshes have been generated employing the GMSH software [30] and are constituted, on average, by approximately 95.000 nodes, and hence 190.000 triangular elements. The number of mesh nodes equals the rank of the (sparse) complex linear system to be solved in order to find the nodal values of the magnetic vector potential (quasi-magnetostatic problem). The solution of the linear system is performed using the Fortran 90 version of the Intel MKL Pardiso library [31] for sparse complex non-symmetric linear systems. As mentioned in Sec. 3.3, a total of 27 characteristic matrices (hence 2D meshes) have been employed to discretize the pipeline path and the resistivity longitudinal changes. The configuration adopted in this work features 6 conductors (including the soil) for every mesh. Hence, following the procedure described in Sec. II, 6 different runs must be performed for each of the 27 meshes in order to extract the corresponding characteristic matrices, for a total of 162 runs of the described quasi-magnetostatic code. Every run takes approximately $1.5\,\mathrm{s}$ on an Intel i7-7700 HQ processor with 16.0 GB of RAM, yielding a total run time of $4\,\mathrm{min}$ for the computation of the characteristic matrices. Once these have been obtained, the equivalent

circuit is built and solved using a MATLAB implementation of the Tableau Analysis methodology (as described in Sec. 2.2). The process of automatically building and solving the equivalent circuit takes approximately 3 s. It should be considered that the most time-intensive process, i.e., the characteristic matrix collection, must be carried out only once for a given geometry (if the materials physical properties are not changed).

5. Conclusion

A quasi-3D methodology, based on the combination of 2D FEA and network analysis, has been employed to analyse the AC interference induced on a buried metallic pipeline by a high voltage power line. Several examples of parallel and nonparallel routings of the two structures have been considered, to assess the physical effects caused by nonuniformities of the soil electrical resistivity over the length of a corridor. The results obtained with the developed quasi-3D methodology show good agreement with the well established approach described in the CIGRE Guide on the Influence of High Voltage AC Power Systems on Metallic Pipelines. With respect to the CIGRE approach, the proposed method can be also emplyed to model configurations comprising multiple earth-return conductors, such as mitigation wires or OGWs. The results provided in Sec. 3 show that longitudinal nonuniformities in the electrical resistivity of the soil can significantly alter the induced current values. The performed simulations have shown that whenever the pipeline is the only earth-return conductor, a highly resistive section of soil has a mitigating effect on the induced current. However, if another earth-return conductor is added, such as an overhead ground wire, the highly resistive soil causes then the induced current on the pipeline to increase. This behaviour has been discussed for both a pipeline running parallel to the power line, and a corridor where the pipeline crosses the power line. The presented methodology allows one to predict the changes of induced voltages and currents produced by soil nonuniformities along the corridor route, and can be used as a modelling tool for mitigation design. Finally, while the physical

configurations assessed in this work are rather simple, the FEM-based nature of the presented methodology also allows taking into account soil resistivity changes in each 2D plane adopted in the finite element calculations, including horizontal layers,vertical layers and arbitrary 2D resistivity distributions. These can be combined with the the longitudinal resistivity gradients presented in this work, to assess the effects of soil resistivity changes in the three physical dimensions.

References

[1] A. W. Peabody, A. L. Verhiel, The effects of high-voltage AC transmission lines on buried pipelines, IEEE Transactions on Industry and General Applications IGA-7 (3) (1971) 395–402.

[2] Corrosion of metals and alloys - Determination of AC corrosion - Protection criteria, Standard EN ISO 18086:2017, International Organization for Standardization (2017).

[3] N. M. Abdel-Gawad, A. Z. E. Dein], M. Magdy, Mitigation of induced voltages and ac corrosion effects on buried gas pipeline near to OHTL under normal and fault conditions, Electric Power Systems Research 127 (2015) 297 – 306. doi:https://doi.org/10.1016/j.epsr.2015.06.007.

[4] Effects Of Electromagnetic Interference On Pipelines Caused By High Voltage A.C. Electric Traction Systems And/or High Voltage A.C. Power Supply Systems , Standard EN 50443:2011, CENELEC - EUROPEAN COMMITTEE FOR STDS - ELECTRICAL (2011).

[5] CEN EN 15280, Evaluation of a.c. corrosion likelihood of buried pipelines applicable to cathodically protected pipelines, (CEN EN 15280) (August 2013).

[6] A. Cristofolini, A. Popoli, L. Sandrolini, Numerical modelling of interference from ac power lines on buried metallic pipelines in presence of mitigation wires, in: 2018 IEEE International Conference on Environment and

Electrical Engineering and 2018 IEEE Industrial and Commercial Power Systems Europe (EEEIC/I&CPS Europe), Palermo, Italy, 2018, pp. 1–6. doi:10.1109/EEEIC.2018.8493677.

[7] A. Popoli, L. Sandrolini, A. Cristofolini, Finite element analysis of mitigation measures for ac interference on buried pipelines, in: 2019 IEEE International Conference on Environment and Electrical Engineering and 2019 IEEE Industrial and Commercial Power Systems Europe (EEEIC / I CPS Europe), 2019, pp. 1–5. doi:10.1109/EEEIC.2019.8783843.

[8] J. Dabkowski, How to predict and mitigate A. C. voltages on buried pipelines., Pipeline and Gas Journal 206 (3) (1979) 19–21.

[9] A. Taflove, J. Dabkowski, Prediction Method for Buried Pipeline Voltages Due to 60 Hz AC Inductive Coupling Part I-Analysis, IEEE Transactions on Power Apparatus and Systems PAS-98 (3) (1979) 780–787. doi:10.1109/TPAS.1979.319290.

[10] F. P. Dawalibi, R. D. Southey, Analysis of electrical interference from power lines to gas pipelines. I. Computation methods, IEEE Transactions on Power Delivery 4 (3) (1989) 1840–1846. doi:10.1109/61.32680.

[11] A. Cristofolini, A. Popoli, L. Sandrolini, A comparison between Carsons formulae and a 2D FEM approach for the evaluation of AC interference caused by overhead power lines on buried metallic pipelines, Progress in Electromagnetics Research C 79 (2017) 39–48. doi:10.2528/PIERC17080501.

[12] G. Lucca, Mutual impedance between an overhead and a buried line with earth return, in: Ninth International Conference on Electromagnetic Compatibility, 1994. (Conf. Publ. No. 396), 1994, pp. 80–86. doi:10.1049/cp:19940679.

[13] A. Ametani, T. Yoneda, Y. Baba, N. Nagaoka, An investigation of earth-return impedance between overhead and underground conductors and

its approximation, IEEE Transactions on Electromagnetic Compatibility 51 (3) (2009) 860–867.

[14] J. R. Carson, Wave propagation in overhead wires with ground return, Bell system technical journal 5 (4) (1926) 539–554. doi:10.1002/j.1538-7305.1926.tb00122.x.

[15] F. Pollackzek, On the field produced by an infinitely long wire carrying alternating current, Elekztrische Nachtrichten Technik (1926).

[16] A. Popoli, L. Sandrolini, A. Cristofolini, A quasi-3D approach for the assessment of induced AC interference on buried metallic pipelines, International Journal of Electrical Power and Energy Systems 106 (May) (2019) 538–545. doi:10.1016/j.ijepes.2018.10.033.

[17] A. Popoli, A. Cristofolini, L. Sandrolini, A numerical model for the calculation of electromagnetic interference from power lines on nonparallel underground pipelines, Mathematics and Computers in Simulation (2020). doi:https://doi.org/10.1016/j.matcom.2020.02.015.

[18] E. H. Enrique, J. D. Walsh, Analysis of touch potentials in solar farms, IEEE Transactions on Industry Applications 51 (5) (2015) 4291–4296.

[19] M. Nakagawa, A. Ametani, K. Iwamoto, Further studies on wave propagation in overhead lines with earth return: impedance of stratified earth, in: Proceedings of the Institution of Electrical Engineers, no. 12, 1973, pp. 1521–1528.

[20] G. Lucca, AC interference from a faulty power line on nearby buried pipelines: Influence of the surface layer soil, IET Science, Measurement and Technology 14 (2) (2020) 225–232. doi:10.1049/iet-smt.2019.0133.

[21] G. C. Christoforidis, D. P. Labridis, P. S. Dokopoulos, Inductive interference on pipelines buried in multilayer soil due to magnetic fields from nearby faulted power lines, IEEE Transactions on Electromagnetic Compatibility 47 (2) (2005) 254–262. doi:10.1109/TEMC.2005.847399.

[22] D. D. Micu, G. C. Christoforidis, L. Czumbil, AC interference on pipelines due to double circuit power lines: A detailed study, Electric Power Systems Research 103 (2013) 1 – 8. doi:https://doi.org/10.1016/j.epsr.2013.04.008.

[23] F. P. Dawalibi, F. Donoso, Integrated analysis software for grounding, EMF, and EMI, IEEE Computer Applications in Power 6 (2) (1993) 19–24. doi:10.1109/67.207467.

[24] CIGRE, Guide on the Influence of High Voltage AC Power Systems on Metallic Pipelines, Tech. rep., Cigré Working Group 36.02 (1995).

[25] C. W. Steele, Numerical computation of electric and magnetic fields, Springer Science & Business Media, 2012.

[26] T. Hayashi, Y. Mizuno, K. Naito, Study on Transmission-Line Arresters for Tower With High Footing Resistance, IEEE Transactions on Power Delivery 23 (4) (2008) 2456–2460.

[27] P. Yadee, S. Premrudeepreechacharn, Analysis of Tower Footing Resistance Effected Back Flashover Across Insulator in a Transmission System, International Conference on Power Systems Transients (2007).

[28] G. Christoforidis, D. Labridis, P. Dokopoulos, N. Kioupis, AC Interference on a Gas Pipeline Caused by Nearby Power Lines in a Copmplex Right-of-way - Comparison between measurements and calculations (Jun.) (2004) 1–15.

[29] R. Djekidel, S. A. Bessedik, P. Spiteri, D. Mahi, Passive mitigation for magnetic coupling between hv power line and aerial pipeline using PSO algorithms optimization, Electric Power Systems Research 165 (2018) 18 – 26. doi:https://doi.org/10.1016/j.epsr.2018.08.014.

[30] C. Geuzaine, J.-F. Remacle, Gmsh: a three-dimensional finite element mesh generator with built-in pre-and post-processing facilities, in: Proceedings of the Second Workshop on Grid Generation for Numerical Computations, Tetrahedron II, 2007.

[31] O. Schenk, K. Gärtner, Solving unsymmetric sparse systems of linear equations with PARDISO, Future Generation Computer Systems 20 (3) (2004) 475–487.